## Sandra Vinnikova

School of Mechanical & Aerospace Engineering, Oklahoma State University, Stillwater, OK 74078 e-mail: sandra.vinnikova@okstate.edu

## Hui Fang

Assistant Professor
Department of Electrical & Computer Engineering,
Northeastern University,
Boston, MA 02115
e-mail: h.fang@northeastern.edu

## Shuodao Wang<sup>1</sup>

Mem. ASME Associate Professor School of Mechanical & Aerospace Engineering, Oklahoma State University, Stillwater, OK 74078 e-mail: shuodao.wang@okstate.edu

# Mechanics of Regular-Shape Nanomeshes for Transparent and Stretchable Devices

Open nanomesh structures with nano/micro-scale geometric dimensions are important candidates for transparent, soft, and stretchable microelectrodes. This study developed analytical and numerical mechanics models for three types of nanomeshes that consist of regular polygons and straight traces. The analytical models described the transparency, effective stiffness, and stretchability of the nanomeshes and agree with the finite element analysis. The mechanical performances of the nanomeshes are compared based on the same level of transparency. The validated analytical expressions provide convenient guidelines for designing the nanomeshes to have levels of transparency and mechanical properties suitable for bio-integrated applications. [DOI: 10.1115/1.4047777]

Keywords: nanomesh, stretchable microelectrodes, effective modulus, stretchability

#### 1 Introduction

Flexible and stretchable electronics plays a critical role in the development of wearable electronic devices. For the past decade, great progress has been achieved in the area of bio-inspired electronics. Examples include electronic eye cameras [1], stretchable organic solar cells [2], flexible displays [3], and artificial sensitive skin [4]. These devices are compatible with bio-integrated applications and can be bent, curved, twisted, compressed, and stretched for biocompatible and medical applications [5].

One of the crucial areas of the application of flexible electronic devices is neuroscience. Mapping physiological electrical activities is a critical element in this area. Neural microelectrode technologies experience a rapid development over the past decades in both fundamental and applied neurosciences [6]. Bioelectronic tools enabled significant advances in the understanding of crucial neuroscience aspects such as memory, behaviors, and decision-making. They also play a significant role in clinical diagnoses of neurological diseases and brain injuries. Neural electrodes can be used to directly read and record brain signals at the cellular level, as well as to provide direct inputs into the brain by employing electrical stimulation paradigms [7].

Currently, solutions that could efficiently perform brain mappings are very limited due to the challenging demand of simultaneous measurement of the current flows from neurons and imaging the cell morphology. A possible approach to overcome this difficulty is to design a transparent electrode that could combine functional electrical, mechanical, and optical properties simultaneously. Mechanically, the electrodes need to be soft so that they can conform to the very complex surfaces of the brain; they should also have a high level of stretchability such that they can overcome large deformation associated with conforming onto complex surface morphologies. Mesh forms of various metals demonstrated high stretchability and flexibility along with transparency, which makes them promising structures for soft bioelectronics [8-13]. Mechanical properties such as effective moduli and Poisson's ratios of architected 2D structures presented by Yang et al. [14], but the mesh structures are different and the objectives focus mainly on elastic and geometric properties. Other studies on architected or metamaterials aimed at achieving high stiffness [15–17], programmable mechanical properties [18–20], or tunable optical/photonic features [21,22].

The purpose of this study is to understand the interplay of various properties of nanomeshes including their transparency, stiffness, and stretchability for microelectrode applications. The desirable nanomesh electrode should meet both the optical and mechanical requirements so that both brain electrophysiology and optical imaging can be achieved [8].

To achieve uniformly distributed sensing capability, it is desirable to have meshes that consist of regular geometries. Filling a 2D plane with regular unit cells is analogous to the Euclidean plane tessellations [23] by convex regular polygons. There exist only three regular tessellations: filling the 2D plane with equilateral (regular) triangles, squares, or hexagons. Analytical and numerical models are presented in this study for the transparency and deformation of the three regular-shape geometries as shown in Fig. 1. The strain distribution and deformation of these structures are obtained analytically and compared to finite element analysis (FEA) results, based on which the transparency, stiffness, and stretchability of the three types of nanomeshes are calculated and compared. These results provide design guidelines for regular-shape nanomesh structures and devices.

#### 2 The Transparency of Nanomeshes

It is critical to compare the performance of the nanomeshes based on a certain standard. From a practical point of view, the transparency of these nanomeshes is one of the critical desirable features. Therefore, it is of interest to analyze the transparency of the structures in Fig. 1. The transparency of the nanomeshes is governed by the ratio of the open area (the area not covered by the metal traces) over the total area. From the geometric analysis, the transparencies of the three types of meshes are found to be

$$T_{\text{tri}} = \left(1 - \frac{\sqrt{3}t_1}{l_1}\right)^2 \tag{1}$$

$$T_{\rm sqr} = \left(1 - \frac{t_2}{l_2}\right)^2 \tag{2}$$

<sup>&</sup>lt;sup>1</sup>Corresponding author.

Contributed by the Applied Mechanics Division of ASME for publication in the JOURNAL OF APPLIED MECHANICS. Manuscript received June 27, 2020; final manuscript received July 1, 2020; published online July 27, 2020. Assoc. Editor: Yonggang Huang.

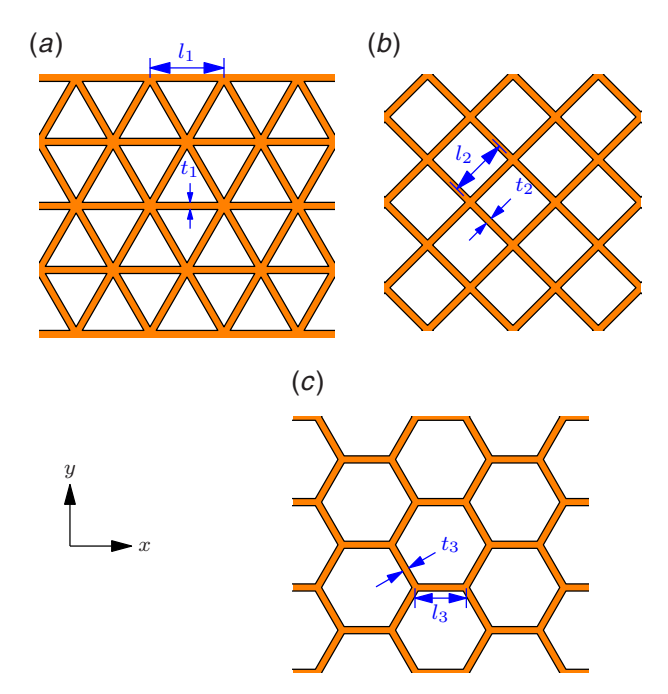


Fig. 1 The three types of regular-shape nanomeshes analogous to the three types of regular Euclidean tessellations: (a) triangular, (b) square, and (c) hexagonal nanomeshes

$$T_{\text{hex}} = \left(1 - \frac{0.5t_3}{l_3}\right)^2 \tag{3}$$

where  $T_{\rm tri}$ ,  $T_{\rm sqr}$ , and  $T_{\rm hex}$  denote the transparency factors of the triangular, square, and hexagonal meshes, respectively, and  $l_i$  are the lengths of traces and  $t_i$  are the in-plane trace widths, as shown in Fig. 1. To achieve the same level of transparency, it is required that

$$\frac{\sqrt{3}t_1}{l_1} = \frac{t_2}{l_2} = \frac{0.5t_3}{l_3} = \alpha \tag{4}$$

where  $\alpha$  is a universal width-to-length ratio such that for the same  $\alpha$ , the three types of nanomeshes will have the same transparency.

It should be noted that in experiments the transparencies of the nanomeshes will also be affected by the thickness of the metal layer and the transparency of the handling substrate; however, as long as the vertical stacking structure design is the same, the transparency of the nanomesh will still be governed by Eqs. (1)–(3).

Now, under the same  $\alpha$  value, the three types of nanomeshes will have the same transparency, and therefore, their mechanical properties can be fairly compared in Sec 3.

## 3 Mechanical Stiffness and Stretchability of the Nanomeshes

The nanomesh structures are considered as interconnected straight beams. The forces of each beam are analyzed based on symmetry and displacement compatibility. The relations between the overall stretching force, the overall deformation, and the maximum strain in the structure are obtained analytically and used to calculate the effective modulus and the stretchability.

**3.1 Mechanical Properties of Triangular Nanomeshes.** The deformation of the triangular nanomesh can be represented by a unit cell shown in Fig. 2(a). Beam EF deforms by the same amount as Beam BC; therefore, it is equivalent to move Beam EF and make its two ends connected with nodes B and C as shown in Fig. 2(b).

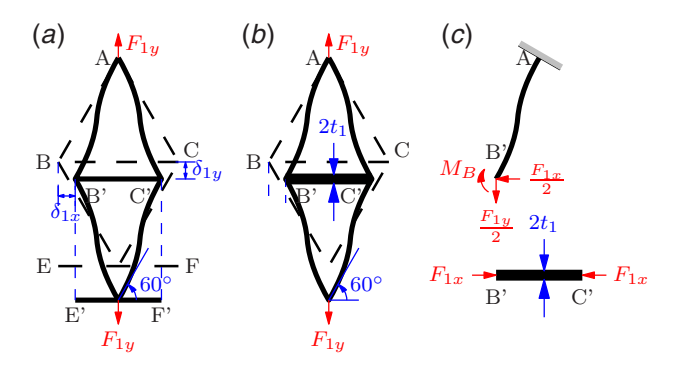


Fig. 2 The mechanical model for the triangular nanomesh: (a) undeformed (dashed lines) and deformed (solid lines) shapes of a unit cell, (b) an equivalent unit cell with Beam BC's width doubled to  $2t_1$ , and (c) internal force analysis of case b

(Beam BC has a thickness of  $2t_1$ .) The internal force analysis of Case b is shown in Fig. 2(c).

The total axial and transverse forces at point B' shown in Fig. 2(c), respectively, as follows:

$$P = \frac{F_{1y}}{2}\cos 30^{\circ} + \frac{F_{1x}}{2}\sin 30^{\circ}$$
 (5)

and

$$Q = \frac{F_{1y}}{2}\sin 30^{\circ} - \frac{F_{1x}}{2}\cos 30^{\circ}$$
 (6)

It is noted that after deformation, all the tangent lines at the junctions remain 60 deg from the horizontal direction, so for deformation compatibility, the total rotation  $\theta_B$  at point B caused by Q and  $M_B$  is zero, i.e.,

$$\theta_B = \frac{Ql_1^2}{2EI_1} - \frac{M_B l_1}{EI_1} = 0$$

therefore

$$M_B = \frac{Ql_i}{2}$$
 (*i* = 1, 2, 3) (7)

Equation 7 is universal to all the angled beams analyzed in this study because the ends of the beams do not rotate.

The total horizontal deflection  $\delta_{1x}$  calculated from Beam AB is:

$$\delta_{1x} = \frac{-Pl_1}{Et_1} \sin 30^\circ + \frac{Ql_1^3}{3EI_1} \cos 30^\circ - \frac{M_B l_1^2}{2EI_1} \cos 30^\circ \tag{8}$$

where *E* is the effective modulus of the beam and  $I_i = t_i^3/12(i = 1, 2, 3)$  is the second moment of inertia per unit out-of-plane thickness.  $\delta_{1x}$  can also be calculated from beam BC:

$$\delta_{1x} = \frac{F_{1x}}{E(2t_1)} \cdot \frac{l_1}{2} \tag{9}$$

The total deflection in the y-direction is

$$\delta_{1y} = \frac{Pl_1}{Et_1} \cos 30^\circ + \frac{Ql_1^3}{3EI_1} \sin 30^\circ - \frac{M_B l_1^2}{2EI_1} \sin 30^\circ \tag{10}$$

and the applied strain  $\epsilon_{\rm app}$  in the y-direction is

$$\epsilon_{\rm app} = \frac{\delta_{1y}}{\frac{\sqrt{3}}{2}l_1} \tag{11}$$

and the maximum strain  $\epsilon_{1\text{max}}$  occurs in Beam AB and

$$\epsilon_{1\text{max}} = \frac{P}{Et_1} - \frac{M_B t_1}{2EI_1} + \frac{Q l_1 t_1}{2EI_1}$$
 (12)

Solving Eqs. (5)–(12) yields

$$\epsilon_{1\text{max}} = \epsilon_{\text{app}} \frac{1 + \frac{2l_1^2}{t_1^2} + \frac{3\sqrt{3}l_1}{t_1}}{1 + \frac{3l_1^2}{t_1^2}}$$
(13)

and the effective modulus of the triangular nanomesh is

$$E_{1y-\text{eff}} = \frac{F_{1y}}{\epsilon_{\text{app}} l_1} = \frac{2\sqrt{3}Et_1}{3l_1} \frac{3 + \frac{3l_1^2}{t_1^2}}{1 + \frac{3l_1^2}{t_1^2}}$$
(14)

When  $\epsilon_{\rm imax}$  reaches the intrinsic fracture strain  $\epsilon_{\rm f}$  of the traces, the corresponding  $\epsilon_{\rm app}$  is defined as the stretchability  $\epsilon_{\rm istr}$  of the nanomeshes  $(i=1,\,2,\,3)$ . Based on Eq. (13), the stretchability is

$$\epsilon_{1\text{str}} = \epsilon_{\text{f}} \cdot \frac{1 + \frac{3l_1^2}{t_1^2}}{1 + 3\sqrt{3}\frac{l_1}{t_1} + \frac{2l_1^2}{t_1^2}}$$
(15)

**3.2** Mechanical Properties of Square Nanomeshes. Applying the same approach for the unit cell shown in Fig. 3(a), the axial and transverse shear forces of Beam AB' (Fig. 3(b)) are as follows:

$$P = Q = \frac{F_{2y}}{2}\cos 45^{\circ} = \frac{\sqrt{2}F_{2y}}{4}$$
 (16)

The total displacement in the y-direction is

$$\delta_{2y} = \frac{Pl_2}{Et_2}\cos 45^\circ + \frac{Ql_2^3}{3EI_2}\cos 45^\circ - \frac{Ml_2^2}{2EI_2}\cos 45^\circ$$
 (17)

and the applied strain is

$$\epsilon_{\rm app} = \frac{\delta_{2y}}{\frac{\sqrt{2}}{2}l_2} \tag{18}$$

The effective modulus of the nanomesh is

$$E_{2y-\text{eff}} = \frac{F_{2y}}{\epsilon_{\text{app}}\sqrt{2}l_2} \tag{19}$$

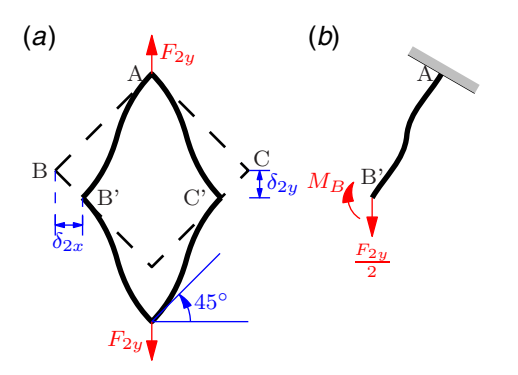


Fig. 3 The mechanical model for the square nanomesh: (a) undeformed (dashed lines) and deformed (solid lines) shapes of a unit cell and (b) internal force analysis

Solving Eqs. (7) and (16)–(19) yields

$$E_{2y-eff} = 2E\left(\frac{l_2}{t_2} + \frac{l_2^3}{t_2^3}\right)^{-1}$$
 (20)

and

$$\epsilon_{2\text{max}} = \epsilon_{\text{app}} \frac{1 + \frac{3l_2}{t_2}}{1 + \frac{l_2^2}{t_2^2}}$$
 (21)

The stretchability of the square nanomesh can be obtained from Eq. (21) as follows:

$$\epsilon_{2\text{str}} = \epsilon_{\text{f}} \cdot \frac{1 + \frac{l_2^2}{t_2^2}}{1 + \frac{3l_2}{t_2}}$$
(22)

**3.3** Mechanical Properties of Hexagonal Nanomeshes. The hexagonal nanomeshes have different properties depending on the stretching directions.

3.3.1 Hexagonal Nanomeshes Stretched in the x-Direction. The model of hexagonal nanomeshes shown in Fig. 4 consists of beams AB, BC, and BD. The axial and transverse shear forces for beam A'B' (Fig. 4(b)) are:

$$P = \frac{F_{3x}}{2} \sin 30^{\circ}$$
 and  $Q = \frac{F_{3x}}{2} \cos 30^{\circ}$  (23)

The total displacement in the *x*-direction is

$$\delta_{3x} = \frac{F_{3x}l_3}{Et_3} + \frac{Pl_3}{Et_3}\sin 30^\circ + \frac{Ql_3^3}{3EI_3}\cos 30^\circ - \frac{Ml_3^2}{2EI_3}\cos 30^\circ$$
 (24)

and the total applied strain is

$$\epsilon_{\rm app} = \frac{\delta_{3x}}{1.5l_3} \tag{25}$$

The effective modulus of the nanomesh is

$$E_{3x-\text{eff}} = \frac{F_{3x}}{\epsilon_{\text{app}}(\sqrt{3}l_3)}$$
 (26)

The maximum strain in the nanomesh is

$$\epsilon_{3\text{xmax}} = \frac{P}{Et_3} + \frac{Ql_3t_3}{2El_3} - \frac{M_Bt_3}{2El_3}$$
 (27)

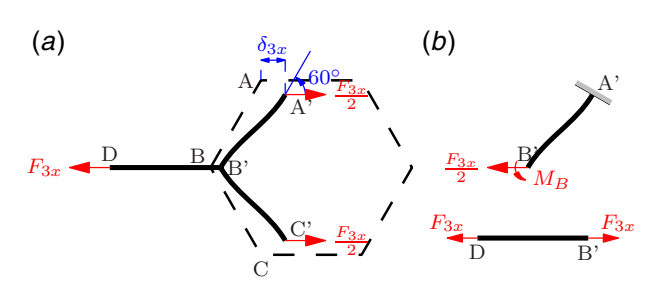


Fig. 4 The mechanical model for the hexagonal nanomesh stretched in the x-direction: (a) undeformed (dashed lines) and deformed (solid lines) shapes of a unit cell and (b) internal force analysis

Solving Eqs. (7) and (23)–(27) yields

$$E_{3x-\text{eff}} = \frac{4\sqrt{3}E}{3} \left(\frac{3l_3}{t_3} + \frac{l_3^3}{t_3^3}\right)^{-1}$$
 (28)

and

$$\epsilon_{3\text{xmax}} = \epsilon_{\text{app}} \frac{1 + \frac{3\sqrt{3}l_3}{t_3}}{3 + \frac{l_3^2}{t_3^2}}$$
(29)

The stretchability is

$$\epsilon_{3xstr} = \epsilon_f \cdot \frac{3 + \frac{l_3^2}{t_3^2}}{1 + \frac{3\sqrt{3}l_3}{t_3}}$$
 (30)

3.3.2 Hexagonal Nanomeshes Stretched in the y-Direction. In this case (Fig. 5), the deformation of the horizontal beams is negligible. The axial and transverse shear forces are as follows:

$$P = F_{3y} \cos 30^{\circ}$$
 and  $Q = F_{3y} \sin 30^{\circ}$  (31)

The total dispalcement in the y-direction is

$$\delta_{3y} = \frac{Pl_3}{Et_3}\cos 30^\circ + \frac{Ql_3^3}{3EI_3}\sin 30^\circ - \frac{Ml_3^2}{2EI_3}\sin 30^\circ$$
 (32)

and the applied strain is

$$\epsilon_{\rm app} = \frac{\delta_{3y}}{\sqrt{3}l_3} \tag{33}$$

The effective modulus is

$$E_{3y-\text{eff}} = \frac{F_{3y}}{\epsilon_{\text{app}}(1.5l_3)} \tag{34}$$

and the maximum strain in the nanomesh is

$$\epsilon_{3\text{ymax}} = \frac{P}{Et_3} + \frac{Ql_3t_3}{2El_3} - \frac{M_Bt_3}{2El_3}$$
(35)

Solving Eqs. (7) and (31)-(35) yields

$$E_{3y-\text{eff}} = \frac{4\sqrt{3}}{3} E \left(\frac{3l_3}{t_3} + \frac{l_3^3}{t_3^3}\right)^{-1}$$
 (36)

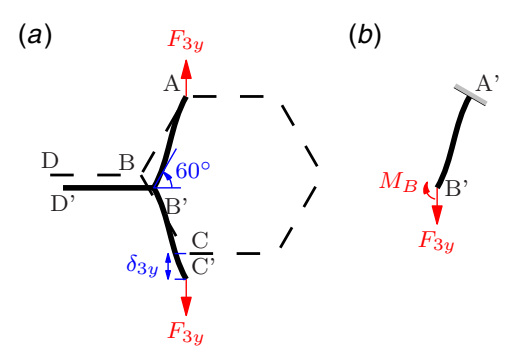


Fig. 5 The mechanical model for the hexagonal nanomesh stretched in the y-direction: (a) undeformed (dashed lines) and deformed (solid lines) shapes of a unit cell and (b) internal force analysis

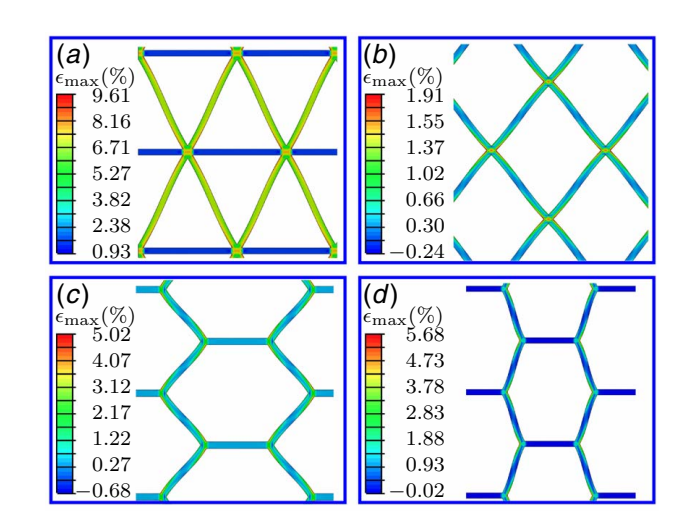


Fig. 6 Finite element modeling results for the (a) triangular nanomesh, (b) square nanomesh, and (c) and (d) hexagonal nanomeshes stretched by 10%. (a)–(c) are stretched in the y-direction and (d) in the x-direction. Only representative areas of the nanomeshes are presented since the deformation is periodic.

and

$$\epsilon_{3\text{ymax}} = \sqrt{3}\epsilon_{\text{app}} \frac{\sqrt{3} + \frac{3l_3}{t_3}}{3 + \frac{l_3^2}{t^2}}$$

$$(37)$$

The stretchability is

$$\epsilon_{3\text{ystr}} = \epsilon_{\text{f}} \cdot \frac{1 + \frac{l_3^2}{3t_3^2}}{1 + \frac{\sqrt{3}l_3}{t_3}}$$
(38)

**3.4 Finite Element Models of the Nanomeshes.** FEA is used to study the three types of nanomeshes. The traces are assumed to have a material modulus of 79 GPa (Young's modulus of thin gold film [24]), and the geometric dimensions are  $t_1 = t_2 = t_3 = 50$  nm,  $l_1 = 866$  nm,  $l_2 = 707$  nm, and  $l_3 = 486$  nm. Each of the nanomeshes is subjected to an applied strain of  $\epsilon_{\rm app} = 10\%$ . The FEA results of deformation and strain distributions are shown in Fig. 6.

The effective moduli and maximum strains in the nanomeshes are calculated in the same way as in the theoretical models. The FEA and theoretical results are tabulated in Tables 1 and 2. The theoretical predictions agree very well with the FEA results.

3.5 Normalized Effective Moduli and Stretchability of the Nanomeshes. The normalized effective moduli and stretchability of the three types of nanomeshes can be expressed by the universal

Table 1 Effective moduli of the nanomeshes

E <sub>eff</sub> (MPa)	FEA	Theory
Triangle	5445	5279
Square	59.1	55.6
Hexagon-x	197.6	192.6
Hexagon-y	197.4	192.6

Table 2 Maximum strain in the nanomeshes under  $\epsilon_{app} = 10\%$ 

$\epsilon_{ m max}$ (%)	FEA	Theory
Triangle	9.61	7.67
Square	1.91	2.16
Hexagon-x	5.02	5.28
Hexagon-y	5.68	5.49

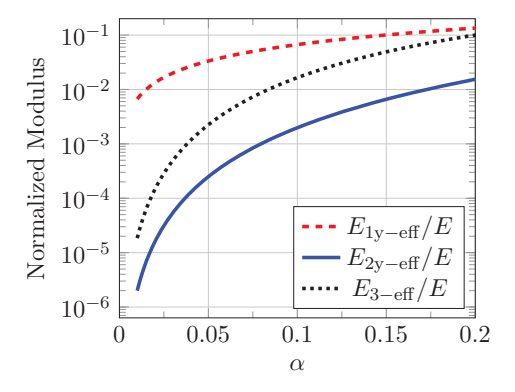


Fig. 7 Normalized effective moduli of the nanomeshes versus  $\alpha$ 

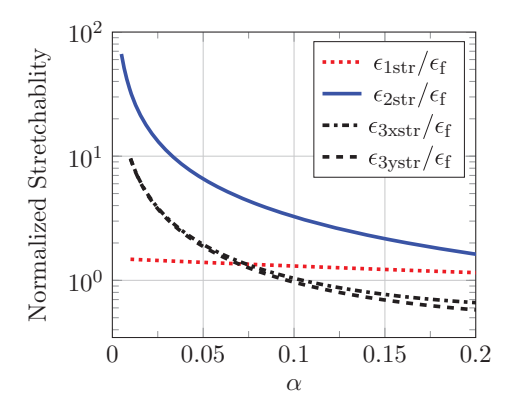


Fig. 8 Normalized stretchability of the nanomeshes versus  $\alpha$ 

width-to-length ratio  $\alpha$  as follows:

$$\frac{E_{1y-\text{eff}}}{E} = \frac{2\alpha^3 + 6\alpha}{\alpha^2 + 9} \qquad \frac{\epsilon_{1y\text{str}}}{\epsilon_f} = \frac{\alpha^2 + 9}{\alpha^2 + 9\alpha + 6}$$

$$\frac{E_{2y-\text{eff}}}{E} = \frac{2\alpha^3}{\alpha^2 + 1} \qquad \frac{\epsilon_{2y\text{str}}}{\epsilon_f} = \frac{\alpha^2 + 1}{\alpha^2 + 3\alpha}$$

$$\frac{E_{3x-\text{eff}}}{E} = \frac{32\sqrt{3}}{3} \frac{\alpha^3}{12\alpha^2 + 1} \qquad \frac{\epsilon_{3x\text{str}}}{\epsilon_f} = \frac{12\alpha^2 + 1}{4\alpha^2 + 6\sqrt{3}\alpha}$$

$$\frac{E_{3y-\text{eff}}}{E} = \frac{32\sqrt{3}}{3} \frac{\alpha^3}{12\alpha^2 + 1} \qquad \frac{\epsilon_{3y\text{str}}}{\epsilon_f} = \frac{12\alpha^2 + 1}{12\alpha^2 + 6\sqrt{3}\alpha}$$
(39)

To compare the nanomeshes' properties based on the same value of  $\alpha$  (the same level of transparency), Eq. (39) is plotted in Figs. 7 and 8.

## 4 Results and Discussion

Based on the aforementioned analyses, the properties of the nanomeshes can be compared based on the same level of transparency. It should be noted first that the triangular nanomesh will only have the properties discussed here when stretched in the *y*-direction,

and similarly, the square nanomesh will be stretchable only in the two diagonal x- and y-directions. Stretching the triangular nanomesh along the x-direction or the square nanomesh along the 45 deg angle as shown in Fig. 1 will result in properties comparable to the intrinsic properties of the traces. The hexagonal nanomeshes, interestingly, have almost the same properties along both x- and y-directions, and the properties in other directions are expected to be similar, resulting in a nearly isotropic mechanical behavior, which is very favorable.

Effective modulus. A typical value of the intrinsic effective modulus of traces is around E=4.2 GPa obtained by a bilayer structure of gold ( $E_{\rm gold}=79$  GPa [24] and 30 nm thick) and polyimide ( $E_{\rm polyimide}=2.0$  GPa [25] and  $1.0\,\mu{\rm m}$  thick). Using this structure and for practical values of  $0.0125 < \alpha < 0.1$  (Fig. 7), the triangular nanomesh's effective modulus is in the range of  $30-300\,{\rm MPa}$  in the y-direction, the square nanomesh is in the range of  $0.01-10\,{\rm MPa}$  along the diagonal directions, and the hexagonal nanomesh is  $0.1-100\,{\rm MPa}$  along any directions. Some of these values are comparable to the elastic modulus of bio-tissues, and they can be further reduced by adopting serpentine traces [26] rather than straight traces

Stretchability. The intrinsic fracture strain of the traces is around  $e_{\rm f} = 5.9\%$  (fracture limit of sub-20 nm gold film [24]). Figure 8 shows that square and hexagonal nanomeshes can boost the stretchability to about ten times larger than  $e_{\rm f}$ , to about 50%, which is already very useful in biocompatible applications. Serpentine traces have a much higher intrinsic fracture strain of ~40% [26] and can be used to achieve stretchability as high as 400% when combined with these nanomesh structures.

### 5 Conclusions

The transparencies and mechanical properties of three types of regular-shape nanomeshes are studied by analytical models that are validated by FEA results. The results showed that for the same level of transparency

- the hexagonal nanomeshes have the best potential as stretchable microelectrodes and exhibit nearly isotropic effective modulus and stretchability that are useful in bio-integrated applications;
- (2) the square nanomeshes have the best mechanical properties (low stiffness, high stretchability) for applications that only require large deformation in one direction or two orthogonal directions; and
- (3) the triangle nanomeshes have high stiffness and low stretchability, so traces with a low intrinsic modulus and a high fracture strain are needed for triangular nanomeshes to be

It should be noted that this study is limited in the sense that only in-plane deformation is considered, which is only accurate when the nanomeshes' out-of-plane thickness is very small so their buckling is restricted by the interfacial adhesion force between the nanomeshes and the bio-tissues. Also, only nanomeshes consist of uniformly distributed regular polygons are considered, which do not allow flexibility in designing structures with macro-scale heterogeneous/anisotropic properties. These issues will need to be addressed in future studies based on their specific applications.

The analytical models presented here provide a convenient toolkit for guiding the designs of regular-shape nanomeshes to achieve levels of transparency, effective modulus, and stretchability that meet the requirements of biocompatible applications. The analytical models can be extended in future studies to account for nanomeshes with curvy traces and of other irregular shapes.

## **Funding Data**

 National Science Foundation (Grants Nos. 1905741 and 1905575; Funder ID: 10.13039/100003187).

#### Conflict of Interest

There are no conflicts of interest.

#### **Data Availability**

The datasets generated and supporting the findings of this article are obtainable from the corresponding author upon reasonable request. The authors attest that all data for this study are included in the paper.

#### References

- [1] Ko, H. C., Stoykovich, M. P., Song, J., Malyarchuk, V., Choi, W. M., Yu, C. -J., Geddes Iii, J. B., Xiao, J., Wang, S., and Huang, Y., et al., 2008, "A Hemispherical Electronic Eye Camera Based on Compressible Silicon Optoelectronics," Nature, 454(7205), pp. 748–753.
- [2] Lipomi, D. J., Tee, B. C. -K., Vosgueritchian, M., and Bao, Z., 2011, "Stretchable Organic Solar Cells," Adv. Mater., 23(15), pp. 1771–1775.
- [3] Jacobs, H. O., Tao, A. R., Schwartz, A., Gracias, D. H., and Whitesides, G. M., 2002, "Fabrication of a Cylindrical Display by Patterned Assembly," Science, 296(5566), pp. 323–325.
- [4] Lumelsky, V. J., Shur, M. S., and Wagner, S., 2001, "Sensitive Skin," IEEE Sens. J., 1(1), pp. 41–51.
- [5] Cheng, T., Zhang, Y., Lai, W.-Y., and Huang, W., 2015, "Stretchable Thin-Film Electrodes for Flexible Electronics With High Deformability and Stretchability," Adv. Mater., 27(22), pp. 3349–3376.
- [6] Guo, Y., Fang, Z., Du, M., Yang, L., Shao, L., Zhang, X., Li, L., Shi, J., Tao, J., Wang, J., Li, H., and Fang, Y., 2018, "Flexible and Biocompatible Nanopaper-Based Electrode Arrays for Neural Activity Recording," Nano Res., 11(10), pp. 5604–5614.
- [7] Kozai, T. D., and Vazquez, A. L., 2015, "Photoelectric Artefact From Optogenetics and Imaging on Microelectrodes and Bioelectronics: New Challenges and Opportunities," J. Mater. Chem. B., 3(25), pp. 4965–4978.
- [8] Seo, K. J., Qiang, Y., Bilgin, I., Kar, S., Vinegoni, C., Weissleder, R., and Fang, H., 2017, "Transparent Electrophysiology Microelectrodes and Interconnects From Metal Nanomesh," ACS Nano, 11(4), pp. 4365–4372.
  [9] Jang, H. Y., Lee, S. -K., Cho, S. H., Ahn, J. -H., and Park, S., 2013, "Fabrication
- [9] Jang, H. Y., Lee, S. -K., Cho, S. H., Ahn, J. -H., and Park, S., 2013, "Fabrication of Metallic Nanomesh: Pt Nano-Mesh as a Proof of Concept for Stretchable and Transparent Electrodes," Chem. Mater., 25(17), pp. 3535–3538.
- [10] Guo, C. F., Liu, Q., Wang, G., Wang, Y., Shi, Z., Suo, Z., Chu, C. -W., and Ren, Z., 2015, "Fatigue-Free, Superstretchable, Transparent, and Biocompatible Metal Electrodes," Proc. Natl. Acad. Sci. USA, 112(40), pp. 12332–12337.
- Electrodes," Proc. Natl. Acad. Sci. USA, 112(40), pp. 12332–12337.
  [11] Miyamoto, A., Lee, S., Cooray, N. F., Lee, S., Mori, M., Matsuhisa, N., Jin, H., Yoda, L., Yokota, T., Itoh, A., Sekino, M., Kawasaki, H., Ebihara, T., Amagai,

- M., and Someya, T., 2017, "Inflammation-Free, Gas-Permeable, Lightweight, Stretchable On-Skin Electronics With Nanomeshes," Nat. Nanotechnol., 12(9), p. 907
- [12] Guo, C. F., Sun, T., Liu, Q., Suo, Z., and Ren, Z., 2014, "Highly Stretchable and Transparent Nanomesh Electrodes Made by Grain Boundary Lithography," Nat. Commun., 5(1), pp. 1–8.
- [13] Trung, T. Q., and Lee, N. -E., 2017, "Materials and Devices for Transparent Stretchable Electronics," J. Mater. Chem. C., 5(9), pp. 2202–2222.
- [14] Yang, W., Liu, Q., Gao, Z., Yue, Z., and Xu, B., 2018, "Theoretical Search for Heterogeneously Architected 2d Structures," Proc. Natl. Acad. Sci. USA, 115(31), pp. E7245–E7254.
- [15] Zheng, X., Lee, H., Weisgraber, T. H., Shusteff, M., DeOtte, J., Duoss, E. B., Kuntz, J. D., Biener, M. M., Ge, Q., Jackson, J. A., Kucheyev, S. O., Fang, N. X., and Spadaccini, C. M., 2014, "Ultralight, Ultrastiff Mechanical Metamaterials," Science, 344(6190), pp. 1373–1377.
- [16] Bauer, J., Schroer, A., Schwaiger, R., and Kraft, O., 2016, "Approaching Theoretical Strength in Glassy Carbon Nanolattices," Nat. Mater., 15(4), pp. 438–443.
- [17] Berger, J., Wadley, H., and McMeeking, R., 2017, "Mechanical Metamaterials at the Theoretical Limit of Isotropic Elastic Stiffness," Nature, 543(7646), pp. 533– 537.
- [18] Coulais, C., Teomy, E., De Reus, K., Shokef, Y., and Van Hecke, M., 2016, "Combinatorial Design of Textured Mechanical Metamaterials," Nature, 535(7613), pp. 529–532.
- [19] Florijn, B., Coulais, C., and van Hecke, M., 2014, "Programmable Mechanical Metamaterials," Phys. Rev. Lett., 113(17), p. 175503.
- [20] Silverberg, J. L., Evans, A. A., McLeod, L., Hayward, R. C., Hull, T., Santangelo, C. D., and Cohen, I., 2014, "Using Origami Design Principles to Fold Reprogrammable Mechanical Metamaterials," Science, 345(6197), pp. 647–650.
- [21] Mousanezhad, D., Babaee, S., Ghosh, R., Mahdi, E., Bertoldi, K., and Vaziri, A., 2015, "Honeycomb Phononic Crystals With Self-Similar Hierarchy," Phys. Rev. B, 92(10), p. 104304.
- [22] Zheludev, N. I., and Plum, E., 2016, "Reconfigurable Nanomechanical Photonic Metamaterials," Nat. Nanotechnol., 11(1), p. 16.
- [23] Grünbaum, B., and Shephard, G., 2013, Tilings and Patterns (Dover Books on Mathematics Series), Dover Publications, Inc., Mineola, New York.
- [24] Lu, Y., Song, J., Huang, J. Y., and Lou, J., 2011, "Fracture of Sub-20 nm Ultrathin Gold Nanowires," Adv. Funct. Mater., 21(20), pp. 3982–3989.
- [25] Zhang, Q., Chen, G., and Zhang, S., 2007, "Synthesis and Properties of Novel Soluble Polyimides Having a Spirobisindane-Linked Dianhydride Unit," Polymer, 48(8), pp. 2250–2256.
- [26] Zhang, Y., Wang, S., Li, X., Fan, J. A., Xu, S., Song, Y. M., Choi, K.-J., Yeo, W.-H., Lee, W., Nazaar, S. N., Lu, B., Yin, L., Hwang, K.-C., Rogers, J. A., and Huang, Y., 2014 ("Experimental and Theoretical Studies of Serpentine Microstructures Bonded to Prestrained Elastomers for Stretchable Electronics," Adv. Funct. Mater., 24(14), pp. 2028–2037.